# Investigations of Zr(IV) in LiF-CaF2: stability with oxide ions and electroreduction pathway on inert and reactive electrodes

Mathieu Gibilaro, Laurent Massot, Pierre Chamelot, Laurent Cassayre, Pierre Taxil

# Investigation of Zr(IV) in $LiF–CaF_2$: Stability with oxide ions and electroreduction pathway on inert and reactive electrodes

M. Gibilaro*, L. Massot, P. Chamelot, L. Cassayre, P. Taxil

*Université de Toulouse, UPS, CNRS, Laboratoire de Génie Chimique, 118 Route de Narbonne, F-31062 Toulouse, France*

A B S T R A C T

In this work, a detailed electrochemical study of the molten $LiF–CaF_2–ZrF_4$ system is provided in the 810–920 °C temperature range, allowing the determination of the reduction potential, the diffusion coefficient and the reduction mechanism of dissolved Zr(IV) on an inert Ta electrode. Addition of CaO in the molten salt is shown to cause Zr(IV) precipitation into an equimolar mixture of solid compounds, most likely $ZrO_2$ and $ZrO_{1.3}F_{1.4}$. Underpotential deposition of Zr on Cu and Ni electrodes is also evidenced and Gibbs energy of formation of Cu–Zr compounds calculated by open circuit chronopotentiometry.

*Keywords:*
Electrochemistry
Zirconium
Molten fluoride
Zirconium oxifluorides
Zr–Cu intermetallic compounds

## 1. Introduction

Pyrochemical route for partitioning and transmutation strategy is considered as one of the most promising option for nuclear fuel cycle, and molten salt electrorefining is well adapted for metallic spent fuel reprocessing, such as U–Zr and U–Pu–Zr [1–3], where the classical hydrometallurgical processes are no more efficient due to the zirconium element. Its presence in the molten bath is commonly considered as an annoyance to the actinide-lanthanide separation, as the zirconium (IV) reduction potential is more positive than uranium in chloride [4–7] and in fluoride salts [8–10], interfering in the actinides selective recovery [11]. In the specific case of molten fluoride solvents, a good knowledge of both $ZrF_4$ chemistry and electrochemistry is thus required.

$ZrF_4$ is mainly prepared by chemical reaction between zirconium oxide $ZrO_2$ and a fluorinating agent, such as fluorine gas [12], hydrogen fluoride [13], ammonium bifluoride [14] or bromium trifluoride [15]. These syntheses evidence the existence of a great number of zirconium oxifluorides solid phases. A full description of the $ZrO_2–ZrF_4$ phase diagram is given by Perpiernik et al., who gathered data for the whole system [16].

The zirconium electrochemical behaviour, in the form of chloride, has been widely investigated and no consensus on its reduction pathway in chloride melts has been found yet. Authors reported several oxidation states (0, +I, +II and +IV) due to a complex chemistry in chloride and in chloro-fluoride melts [17–19].

To obtain a less hygroscopic form and to decrease Zr(IV) volatility [20], numerous studies have been performed on the fluoride form, $ZrF_4$, and were devoted to the deposition in fluoride media of coherent Zr metal and Zr alloys preparation on Ni, B and C [8,21–25]. In these media, the electrochemical reduction of Zr(IV) is a one-step process exchanging 4 electrons, as it has been proved by many authors [9,10] and more recently demonstrated in LiF–NaF by Groult et al. [8]. Anyway, no study has been performed yet in $LiF–CaF_2$ medium.

This paper presents a detailed electrochemical study of Zr(IV) ions behaviour in $LiF–CaF_2$ in the 810–920 °C temperature range on inert electrode (Ta) using several electrochemical techniques (cyclic and square wave voltammetries, chronopotentiometry). Very sensitive to oxide, oxide ions (CaO) have been added into the $LiF–CaF_2–ZrF_4$ mixture to investigate the zirconium precipitation by formation of Zr–O–F solid phases. Finally, Zr(IV) has been deposited on reactive electrodes (Ni, Cu) and, after determination of phases composition by EDS–SEM, the Gibbs energy of formation of these intermetallic compounds were estimated by open circuit chronopotentiometry on the Cu–Zr system. The experimental data were compared to existing thermochemical data.

## 2. Experimental

The cell was a vitreous carbon crucible placed in a cylindrical vessel made of refractory steel and closed by a stainless steel lid cooled by circulating water. The inside part of the walls was protected against fluoride vapours by a graphite liner. The experiments were performed under an inert argon atmosphere (less than one ppm $O_2$), previously dehydrated and deoxygenated using a

* Corresponding author. Tel.: +33 5 61 55 72 19; fax: +33 5 61 55 61 39.
*E-mail address:* gibilaro@chimie.ups-tlse.fr (M. Gibilaro).

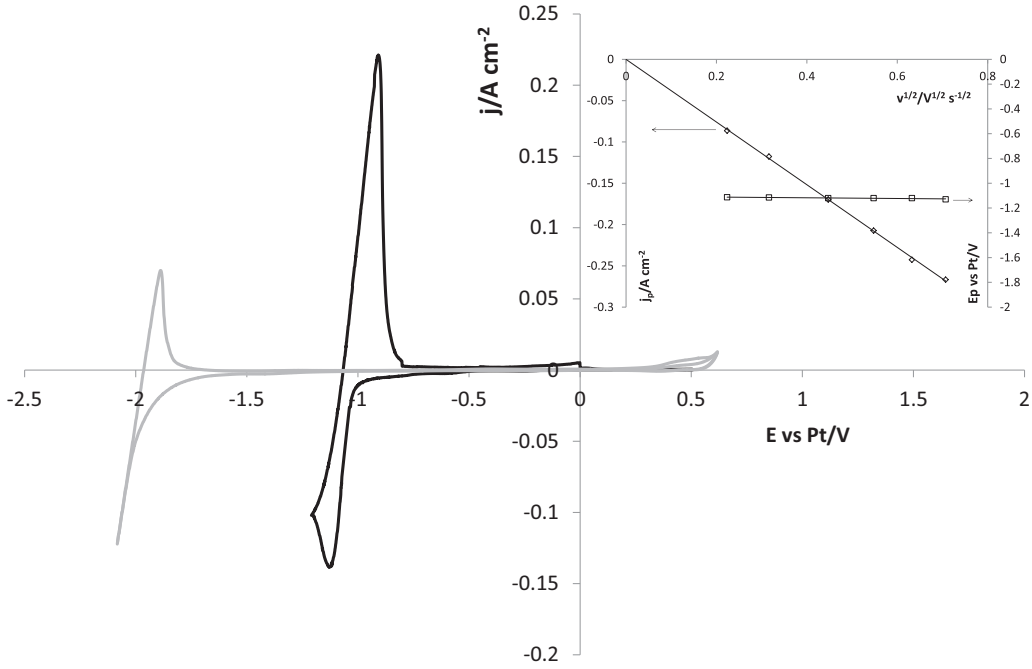


**Fig. 1.** Cyclic voltammograms on Ta of the LiF–$CaF_2$ system at 100 mV $s^{-1}$ and 840 °C: without $ZrF_4$ (grey) and with $ZrF_4$ addition of 0.05 mol $kg^{-1}$ (black). *Inset*. Variation of the peak current density and the peak potential versus the square root of the potential scan rate. Working el.: Ta ($S$ = 0.31 $cm^2$); auxiliary el.: glassy carbon; comparison el.: Pt.

purification cartridge (Air Liquide). The cell was heated using a programmable furnace and the temperatures were measured using a chromel–alumel thermocouple. A more detailed description of the set-up can be found in [26].

The electrolytic bath consisted of a eutectic LiF–$CaF_2$ (Appolo 99.99%) mixture (79.5/20.5 molar ratio), initially dehydrated by heating under vacuum ($10^{-5}$ bar) to its melting point (762 °C) for 72 h. Zirconium ions were introduced into the bath in the form of $ZrF_4$ pellets (Cerac 99.99%) and oxide ions in the form of CaO powder (Cerac 99.9%).

Tantalum, copper and nickel wires (Goodfellow 99.99%, 1 mm diameter) were used as working electrodes. The auxiliary electrode was a vitreous carbon (V25) rod (3 mm diameter) with a large surface area (2.5 $cm^2$).

The potentials were referred to a platinum wire (0.5 mm diameter) immersed in the molten electrolyte, acting as a quasi-reference electrode Pt/$PtO_x$/$O^{2-}$ [27].

The electrochemical study and the electrolyses were performed with an Autolab PGSTAT30 potentiostat/galvanostat controlled with the GPES 4.9 software.

The composition and microstructure of Zr deposits obtained on reactive electrodes were characterized by scanning electron microscope (SEM) coupled with an energy dispersive spectroscopy (EDS) probe.

Cyclic voltammetry, chronopotentiometry, square wave voltammetry and open circuit chronopotentiometry were used for the investigation of the zirconium electroreduction process.

## 3. Results and discussion

### 3.1. Zr(IV) reduction mechanism on inert electrode

#### 3.1.1. $ZrF_4$ in LiF–$CaF_2$

*3.1.1.1. Cyclic voltammetry.* A series of cyclic voltammograms has been plotted on an inert tantalum electrode. A representative voltammogram is presented in Fig. 1 in LiF–$CaF_2$–$ZrF_4$ ($c_0$ = 0.05 mol $kg^{-1}$) at 840 °C and 100 mV $s^{-1}$, where a single peak is observed in the cathodic run at around −1.15 V vs Pt. This peak is associated with a reoxidation peak at around −0.9 V vs. Pt, whose shape is typical of the dissolution of a metal deposited during a cathodic run (stripping peak). As presented in the Fig. 1 inset, the quasi-reversibility of the system, characterized by a peak potential independent of the scan rate, is verified.

The cathodic peak current increased linearly with the concentration of zirconium (IV) ions (Fig. 2), confirming that this peak can be attributed to the Zr(IV) reduction reaction.

Then, the influence of the scan rate on the peak current was studied (Fig. 1 inset) to verify the Berzins Delahaye relationship, valid for a reversible soluble/insoluble system and a diffusion-controlled reaction [28]:

$$I_p = -0.61nFSc_0\left(\frac{nF}{RT}\right)^{1/2} D^{1/2}\upsilon^{1/2} \quad (1)$$

where $n$ is the number of exchanged electrons, $F$ the Faraday constant (96,500 C), $S$ the electrode surface area in $cm^2$, $D$ the diffusion

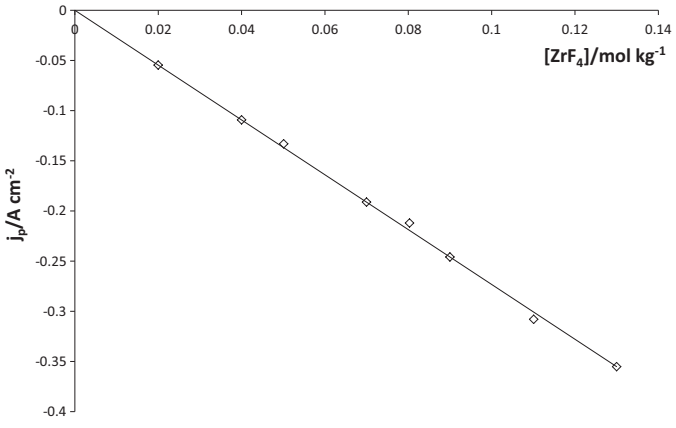


**Fig. 2.** Linear relationship between the cathodic peak current density and the $ZrF_4$ content in the bath in the LiF–$CaF_2$ system on Ta electrode at 100 mV $s^{-1}$ and 840 °C.

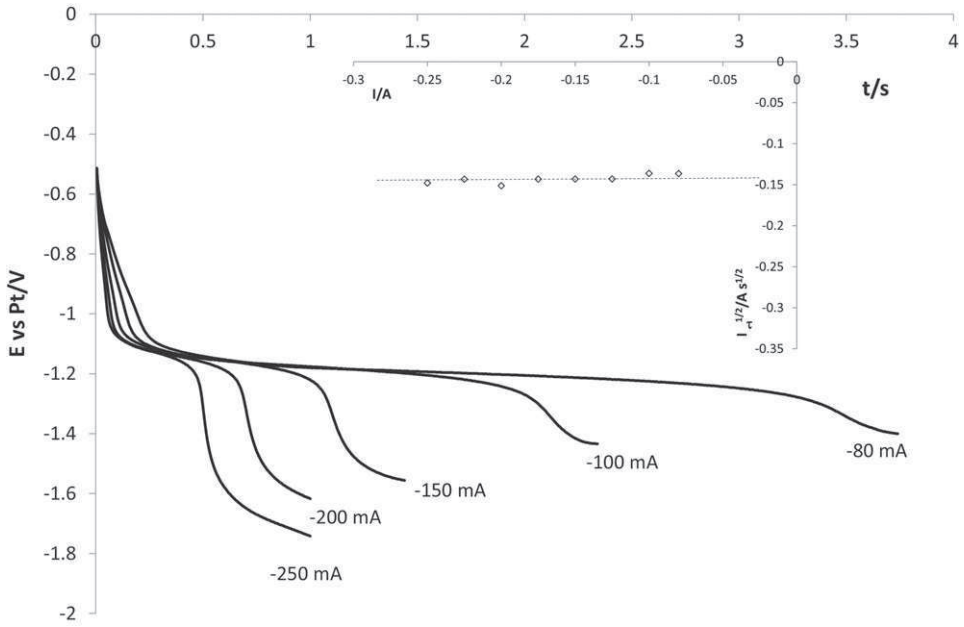


**Fig. 3.** Variation of the chronopotentiograms of the LiF–$CaF_2$–$ZrF_4$ (0.08 mol $kg^{-1}$) system at 840 °C with the applied current on Ta. *Inset*. variation of $I\tau^{1/2}$ vs. the current at 840 °C. Working el.: Ta ($S$ = 0.31 $cm^2$); auxiliary el.: glassy carbon; comparison el.: Pt.

coefficient in $cm^2\,s^{-1}$, $c_0$ the solute concentration in mol $cm^{-3}$, $T$ the absolute temperature in K and $\upsilon$ the potential scan rate in $V\,s^{-1}$.

The linear relationship between $i_p$ and $\upsilon^{1/2}$ observed in the Fig. 1 inset confirms the previous assumptions:

- the reaction yields an insoluble product, likely zirconium metal
- the electrode process is diffusion controlled.

The slope of this linear equation is:

$$\frac{i_p}{\upsilon^{1/2}} = -0.379 \pm 0.002 \quad A\ s^{1/2}V^{-1/2}cm^{-2} \tag{2}$$

at $t$ = 840 °C and $c_0$ = 0.05 mol $kg^{-1}$.

*3.1.1.2. Chronopotentiometry.* Chronopotentiometry was performed on Ta at 840 °C to confirm that the electrochemical process is controlled by zirconium ions diffusion in the melt. In Fig. 3, chronopotentiograms plotted at various current densities at 0.08 mol $kg^{-1}$ exhibit a single plateau at about −1.15 V vs Pt corresponding to the potential of the Zr(IV) reduction into Zr metal evidenced in Fig. 1. The transition time $\tau$ decreased when the applied current increased, in good accordance with the Sand's law [29] valid for diffusion-controlled reactions:

$$\frac{i\tau^{1/2}}{c_0} = 0.5n\pi^{0.5}FD^{0.5} \tag{3}$$

where $\tau$ is the transition time in s.

The data plotted in the Fig. 3 inset are not influenced by $c_0$, in accordance with Eq. (3); the validity of this equation was checked in the 810–920 °C temperature range and at 840 °C and the constant value is:

$$\frac{i\tau^{1/2}}{c_0} = -880.8 \pm 0.2 \quad A\ s^{1/2} \tag{4}$$

The reversal chronopotentiogram presented in Fig. 4 ($c_0$ = 0.08 mol $kg^{-1}$ and $I$ = ±150 mA) exhibits an anodic transition time equal to the cathodic one ($\tau_{ox} = \tau_{red}$ = 1.6 s). This result, characteristic of an insoluble compound formation on the electrode, confirms that the reaction yields Zr metal on the working electrode.

*3.1.1.3. Number of exchanged electrons.* The Zr formation by reduction of Zr(IV) in one step at −1.1 V vs Pt was finally evidenced by calculating the number of exchanged electrons during the cathodic process.

Two methods were used for this calculation:

- combination of cyclic voltammetry and chronopotentiometry measurements,
- square wave voltammetry.

The first method allows the uncertainty on the Zr(IV) concentration and diffusion coefficient to be ignored by coupling (1) and (3):

$$\frac{I_p/\sqrt{\upsilon}}{I\sqrt{\tau}} = 74.173\sqrt{\frac{n}{T}} \tag{5}$$

From these equations, the calculated number of exchanged electrons was found to be 3.8 ± 0.2.

The other technique used to determine the number of exchanged electrons is the square wave voltammetry [30]. In this

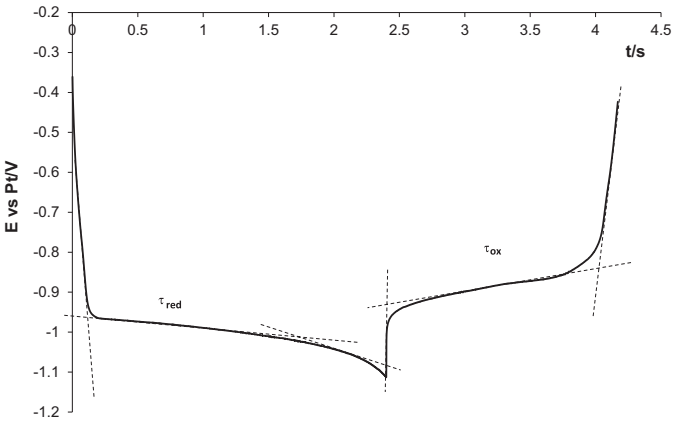


**Fig. 4.** Reversed chronopotentiogram of the LiF–$CaF_2$–$ZrF_4$ (0.08 mol $kg^{-1}$) system at 840 °C; applied current = ±0.15 A. Working el.: Ta ($S$ = 0.31 $cm^2$); auxiliary el.: glassy carbon; comparison el.: Pt.

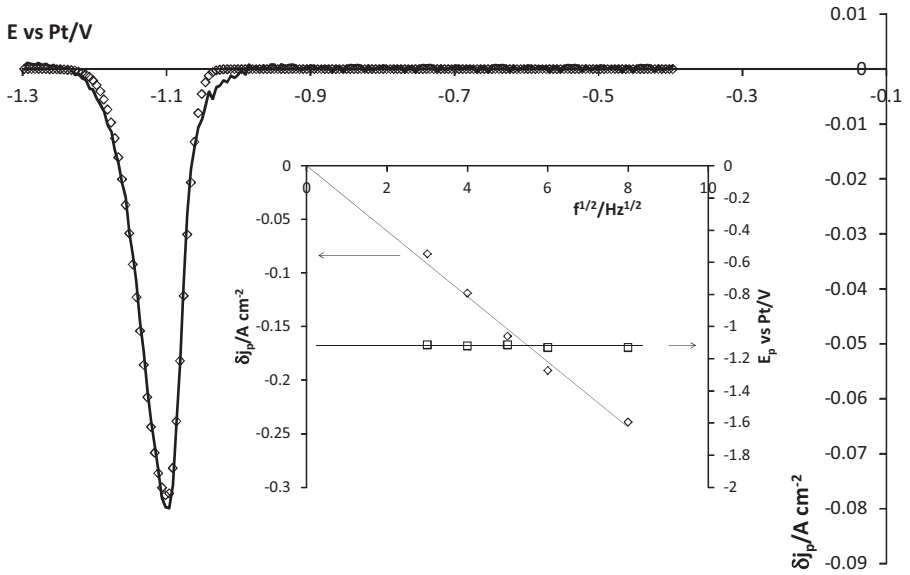


**Fig. 5.** Square wave voltammogram of the LiF–$CaF_2$–$ZrF_4$ (0.05 mol $kg^{-1}$) system at 9 Hz at 840 °C. Black line: deconvoluted signal. *Inset*. Variation of the peak current density and the peak potential versus the square root of the frequency. Working el.: Ta ($S$ = 0.31 $cm^2$); auxiliary el.: glassy carbon; comparison el.: Pt.

method, derived from cyclic voltammetry, the scanning of potential proceeds stepwise with superimposition on each step of the staircase of two potential pulses, direct and reverse, with equal values. Plotting the differential current measured at each step between the successive pulses versus the potential associated to each electrochemical reaction, a Gaussian shaped peak is obtained. In the case of a reversible system, a mathematical analysis of the peak yields a simple equation associating the half-width of the peak ($W_{1/2}$) and the number of exchanged electrons:

$$W_{1/2} = 3.52\frac{RT}{nF} \tag{6}$$

A typical square wave voltammogram in LiF–$CaF_2$–$ZrF_4$ ($c_0$ = 0.05 mol $kg^{-1}$) is shown in Fig. 5 at $T$ = 840 °C and $f$ = 9 Hz. The curve exhibits one peak at about −1.1 V vs Pt corresponding to the $E_{p/2}$ of the cyclic voltammogram. Beforehand, the validity of Eq. (7) was verified in Fig. 5 inset, as far as a linear relationship is obtained between the peak current and the square root of the frequency [31].

As mentioned in previous papers, the distortion of the peak, in comparison with the classical Gaussian peak valid for a soluble/soluble system, is due to the currentless nucleation phase during the metal deposition. Concerning quasi-reversible system with asymmetric peak, the reference [32] indicates how to determine the half-peak width ($W_{1/2}$). From $W_{1/2}$ measurements, the number of exchanged electrons is equal to 4.0 ± 0.1.

Thus, both methods confirm that Zr(IV)/Zr(0) reduction proceeds in a single step, according to:

$$Zr(IV)4e^- = Zr \tag{7}$$

*3.1.1.4. Diffusion coefficient determination.* Using Eq. (1) or (3) and $n$ = 4, the Zr(IV) diffusion coefficient ($D$) was calculated to be $(6.8 \pm 0.1) \times 10^{-6}$ $cm^2$ $s^{-1}$ at 840 °C, whatever the determination method. In the 810–920 °C temperature range, the linear variation of ln $D$ versus the inverse absolute temperature, plotted in Fig. 6, follows an Arrhenius' law as:

$$\ln D = -2.22(\pm 0.03) - \frac{10765.10(\pm 0.03)}{T} \tag{8}$$

From Eq. (8), the activation energy is 89.5 ± 0.2 kJ $mol^{-1}$.

This is in good agreement with the activation energy determined by Groult et al. (76.2 kJ $mol^{-1}$) in a study devoted to the LiF–NaF–$ZrF_4$ system [9].

*3.1.2. $ZrF_4$ in LiF–$CaF_2$–CaO*

Fig. 7 presents cyclic voltammograms plotted on a Ta electrode at 100 mV $s^{-1}$ in LiF–$CaF_2$–$ZrF_4$ (0.11 mol $kg^{-1}$) after successive CaO additions: the Zr(IV) peak current density decreases gradually with the oxide content. After addition of 2.4 mol of CaO, no more electrochemical signal related to the Zr system is observed on Ta.

The normalized quantity of zirconium ions $n$(Zr) has been plotted versus the normalized oxide ions content n(oxide), calculated as:

$$n(\mathrm{Zr}) = \frac{n_{ZrF_4}}{n^0_{ZrF_4}} \quad \text{and} \quad n(\text{oxide}) = \frac{n_{O^{2-}}}{n^0_{ZrF_4}}$$

where $n^0_{ZrF_4}$ is the initial quantity of Zr(IV) in mol, $n_{ZrF_4}$ the remaining quantity of Zr(IV) in mol determined by cyclic voltammetry, $n_{O^{2-}}$ the added quantity of $O^{2-}$ in mol.

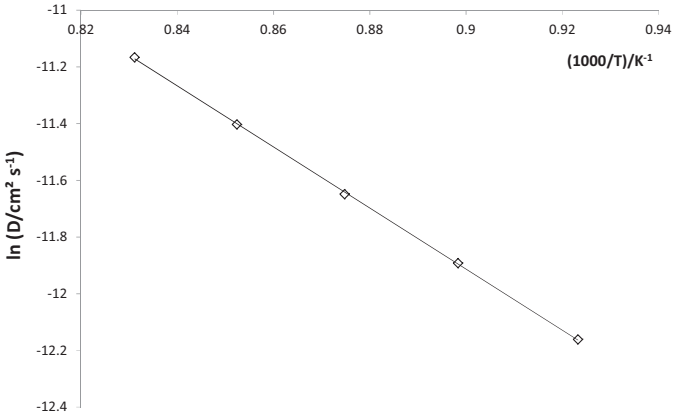


**Fig. 6.** Variation of the logarithm of the diffusion coefficient versus the inverse of the absolute temperature.

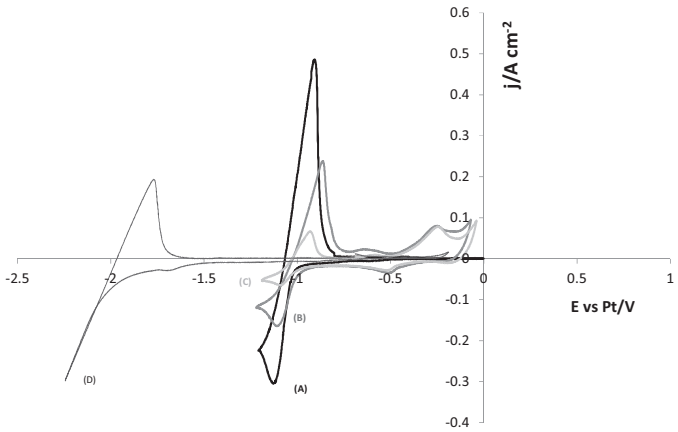


**Fig. 7.** Variation of the cyclic voltammograms of the LiF–$CaF_2$–$ZrF_4$ (0.11 mol $kg^{-1}$) system with oxide ions addition in the solution at 100 mV $s^{-1}$ and 840 °C. (A): before oxide ions addition; (B) oxide ions addition: 0.058 mol $kg^{-1}$; (C) oxide ions addition: 0.143 mol $kg^{-1}$; (D) oxide ions addition: 0.178 mol $kg^{-1}$. Working el.: Ta ($S$ = 0.31 $cm^2$); auxiliary el.: glassy carbon; comparison el.: Pt.

The data, presented in Fig. 8, exhibit a linear relationship between the quantity of added oxide and the decrease of Zr(IV) concentration. As reported in previous work in the case of rare earth [33], this behaviour is an evidence of the formation of a solid compound. The first assumption was that insoluble $ZrO_2$ was formed during oxide additions. However, as evidenced by the theoretical slope of $ZrO_2$ formation plotted in Fig. 8, this assumption does not fit with experimental data. It is thus very likely that oxyfluoride Zr–O–F compounds were formed during the reaction. At the operating temperature (840 °C), according to the $ZrF_4$–$ZrO_2$ phase diagram [16], there are three non-stoichiometric stable oxyfluoride phases: $Zr(F,O)_{4-x}$ ($0.25 < x < 0.34$), $Zr(F, O)_{3+x}$ ($0.33 < x < 0.50$) and $Zr(F, O)_{3-x}$ ($x \sim 0.30$). The composition of these phases is reported in Fig. 8. From these data, it is thus believed that additions of CaO into a $ZrF_4$-containing LiF–$CaF_2$ salt lead to the formation of a close to equimolar mixture of solid $ZrO_2$ and $ZrO_{1.3}F_{1.4}$.

### 3.2. Zr(IV) reduction mechanism on reactive electrode

This section is dedicated to the study of Zr(IV) reduction on reactive cathodes in LiF–$CaF_2$ at 840 °C. Cu and Ni electrodes were selected since both Cu–Zr and Ni–Zr systems present many intermetallic compounds at the operating temperature [34,35].

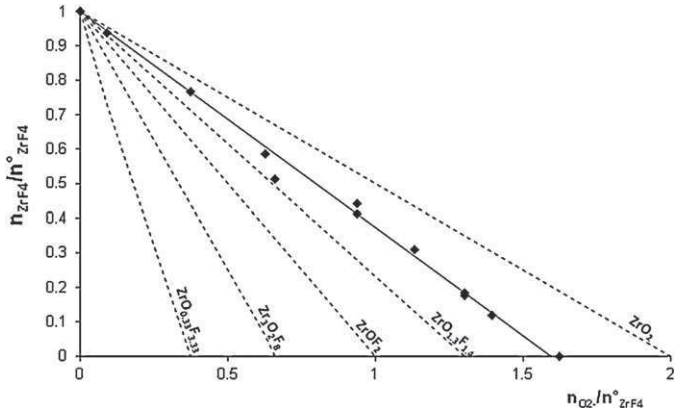


**Fig. 8.** Variation of the normalized Zr(IV) amount in the melt versus the normalized oxide ions content added in the melt. Comparison to existing phases in the Zr–O–F system at 840 °C (1) $Zr(F,O)_{4-x}$ ($0.25 < x < 0.34$) phase; (2) $Zr(F, O)_{3+x}$ ($0.33 < x < 0.50$) phase (3) $Zr(F, O)_{3-x}$ ($x \sim 0.30$) phase.

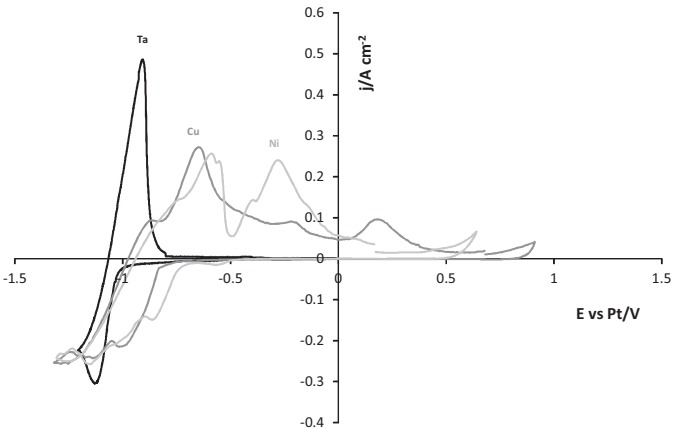


**Fig. 9.** Superposition of the cyclic voltammograms of the LiF–$CaF_2$–$ZrF_4$ (0.11 mol $kg^{-1}$) at 100 mV $s^{-1}$ and 840 °C. Working el.: Ta, Cu, Ni ($S$ = 0.31 $cm^2$); auxiliary el.: glassy carbon; comparison el.: Pt.

#### 3.2.1. Cyclic voltammetry

The cyclic voltammograms presented in Fig. 9 represent zirconium ions reduction on inert (Ta) and on reactive electrodes (Cu, Ni) at 100 mV $s^{-1}$. On both reactive electrodes, additional reduction waves are detected at around -0.85 V vs Pt on Cu and −0.75 V vs Pt on Ni prior to Zr metal deposition on Ta, and are attributed to alloys formation. These shifts in potential are due to a depolarisation effect also called underpotential deposition: the Zr alloy formation occurs at more positive potential than pure Zr [36].

#### 3.2.2. Electrolysis runs

Galvanostatic electrolyses in LiF–$CaF_2$–$ZrF_4$ (0.11 mol $kg^{-1}$) were performed during 30 min at −0.1 A $cm^{-2}$ on Ni and Cu plates. The cross-section of the samples was analyzed by SEM–EDX and micrographs are presented in Fig. 10a (Cu) and b (Ni): several layers of intermetallic compounds are formed at the surface of the electrodes. Their compositions, reported from the inside to the outside of the starting material, are:

- On copper electrode: $Cu/Cu_5Zr/Cu_{51}Zr_{14}/CuZr_2$
- On nickel electrode: $Ni/Ni_5Zr/Ni_{21}Zr_8/NiZr$

Ni–Zr and Cu–Zr alloys have thus been obtained, confirming the underpotential deposition of Zr(IV) ions on reactive cathodes. As previously demonstrated on other systems, it was noticed on both electrodes that the compound with the highest Ni or Cu content is obtained at the boundary of the initial Ni or Cu metal substrates [37].

#### 3.2.3. Gibbs energy calculations using open circuit chronopotentiometry data

Zr-based compounds have been formed and identified after electrolysis runs and open circuit chronopotentiometry was used to determine the Gibbs energy of formation of these compounds. This electrochemical method is however restricted to binary systems containing intermetallic compounds rather than solid solutions. As the Zr–Ni phase diagram exhibits both solid solutions and intermetallic compounds, the determination of Gibbs energy values has been applied to the Cu–Zr system and its 6 intermetallic compounds: $CuZr_2$, CuZr, $Cu_{10}Zr_7$, $Cu_8Zr_3$, $Cu_{51}Zr_{14}$ and $Cu_5Zr$ [34].

The method consists in first electrodepositing a small quantity of Zr on the cathode by a short cathodic run and then measuring the open circuit potential of the cathode versus time. The intermetallic diffusion of Zr and Cu leads to the successive formation of Zr–Cu compounds, with a decreasing Zr content from the surface to the bulk of the Cu material. The open circuit chronopotentiogram then

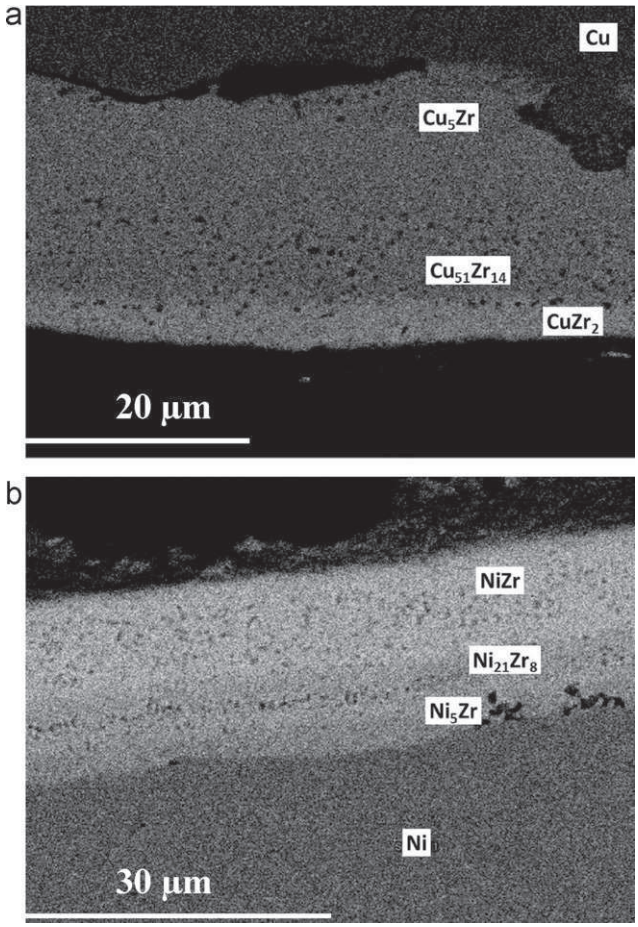


**Fig. 10.** SEM micrographs of a cross section of Cu (a) and Ni (b) plates after reduction of $ZrF_4$ at 840 °C in LiF–$CaF_2$–$ZrF_4$ (0.11 mol kg$^{-1}$). Applied current = −0.1 A cm$^{-2}$, time = 30 min.

exhibits plateaus of metallic interdiffusion corresponding to successive intermetallic compounds formation at the surface of the electrode, as described in [38,39]. Each potential plateau of the chronopotentiogram corresponds to an equilibrium between two intermetallic compounds in the solid state and diffusion of Zr within the substrate explains the cathode potential increase.

The chronopotentiogram of the Cu–Zr system is presented in Fig. 11 where 7 plateaus have been observed on top of pure Zr. By

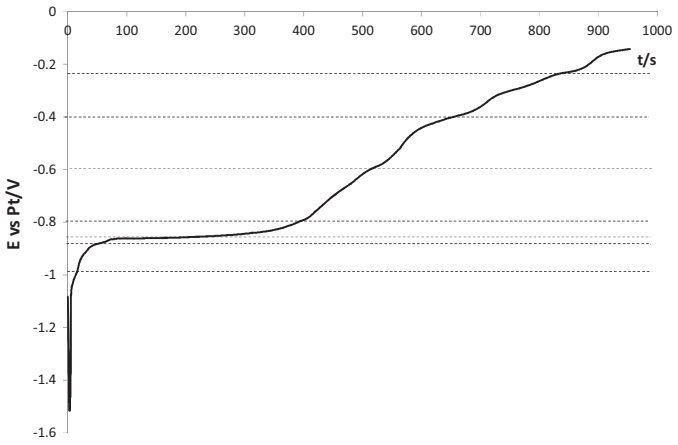


**Fig. 11.** Open-circuit chronopotentiogram of glassy LiF–$CaF_2$–$ZrF_4$ (0.11 mol kg$^{-1}$) on Cu electrode ($S$ = 0.31 cm$^2$) at 840 °C after a polarization at $I$ = −0.2 A. Auxiliary el.: glassy carbon; comparison el.: Pt.

**Table 1**
Experimental values of Gibbs energy of formation compared to calculated one from SGTE database in the Cu–Zr system at 840 °C.

| Compound | $\Delta E$ vs. Zr/V | $\Delta_f G$ (J mol$^{-1}$) | $\Delta_f G_{exp}$ (kJ mol$^{-1}$) | |
|---|---|---|---|---|
| | | | This work | SGTE database |
| Zr | | | | |
| $CuZr_2$ | 0.063 | −24,318 | −24 ± 1 | −38 |
| CuZr | 0.083 | −32,038 | −28 ± 1 | −28 |
| $Cu_{10}Zr_7$ | 0.158 | −60,988 | −258 ± 2 | −242 |
| $Cu_8Zr_3$ | 0.347 | −133,942 | −168 ± 2 | −148 |
| $Cu_{51}Zr_{14}$ | 0.520 | −200,720 | −985 ± 2 | −844 |
| $Cu_5Zr$ | 0.724 | −279,464 | −90 ± 2 | −62 |

linear combination (see reference [39] for calculation details), the Gibbs energy of formation of each intermetallic compound has been calculated. The data are compiled in Table 1. For most compounds, a rather good agreement is found between the present experimental values and the one tabulated in the SGTE database [40].

## 4. Conclusions

The $ZrF_4$ electrochemical behaviour has been investigated in LiF–$CaF_2$ at 840 °C on inert electrode (Ta) and its reduction takes place at around 1 V from the solvent reduction ($Li^+$). Using different electrochemical techniques, it was demonstrated that the reduction mechanism is a one step process exchanging 4 electrons and controlled by the Zr ions diffusion in the molten salt, in accordance with previous studies in molten fluoride solvents: $Zr(IV) + 4e^- = Zr$.

Diffusion coefficients have also been determined on a wide temperature range (810–920 °C) and data show a dependence of ln $D$ with the inverse of the temperature, as a classical Arrhenius-type law:

$$\ln D = -2.22(\pm 0.03) - \frac{10765.10(\pm 0.03)}{T}$$

Then, the effect of oxide ions by CaO addition in a LiF–$CaF_2$–$ZrF_4$ system has been studied. At 850 °C, the zirconium precipitation is evidenced and the concentration decrease of Zr(IV) with CaO additions indicates that the precipitate is most probably composed of zirconium oxide $ZrO_2$ and zirconium oxifluoride $ZrO_{1.3}F_{1.4}$. On nickel and copper electrodes, Zr(IV) reduction was observed at a more positive potential than pure Zr deposition and zirconium alloys formation (Ni–Zr and Cu–Zr) were evidenced by SEM–EDS. Thanks to the open circuit chronopotentiometry data on the Zr–Cu system, the Gibbs energy of formation of the corresponding intermetallic compounds ($CuZr_2$, CuZr, $Cu_{10}Zr_7$, $Cu_8Zr_3$, $Cu_{51}Zr_{14}$, $Cu_5Zr$) were estimated and in good agreement with the SGTE database.

## Acknowledgement

This study was partly financially supported by CNRS within the frame of the French PACEN programme.

## References

[1] T. Koyama, M. Iizuka, Y. Shoji, R. Fujita, H. Tanaka, T. Kobayashi, M. Tokawai, An experimental study of molten salt electrorefining of uranium using solid iron cathode and liquid cadmium cathode for development of pyrometallurgical reprocessing, Journal of Nuclear Science and Technology 34 (1997) 384.
[2] K. Kinoshita, T. Koyama, T. Inoue, M. Ougier, J.P. Glatz, Separation of actinides from rare earth elements by means of molten salt electrorefining with anodic dissolution of U-Pu-Zr alloy fuel, Journal of Physics and Chemistry of Solids 66 (2005) 619.
[3] M. Iizuka, K. Kinoshita, T. Koyama, Modeling of anodic dissolution of U-Pu-Zr ternary alloy in the molten LiCl-KCl electrolyte, Journal of Physics and Chemistry of Solids 66 (2005) 427.
[4] R. Baboian, D.L. Hill, R.A. Bailey, Electrochemical studies on zirconium and hafnium in molten LiCl-KCl eutectic, Journal of the Electrochemical Society 112 (1965) 1221.

[5] Y. Sakamura, Zirconium behavior in molten LiCl-KCl eutectic, Journal of the Electrochemical Society 151 (2004) C187.
[6] S.A. Kuznetsov, H. Hayashi, K. Minato, M. Gaune-Escard, Electrochemical behavior and some thermodynamic properties of UCl4 and UCl3 dissolved in a LiCl-KCl eutectic melt, Journal of the Electrochemical Society 152 (2005) C203.
[7] P. Masset, D. Bottomley, R. Konings, R. Malmbeck, A. Rodrigues, J. Serp, J.P. Glatz, Electrochemistry of uranium in the LiCl-KCl eutectic, Journal of the Electrochemical Society 152 (2005) A1109.
[8] H. Groult, A. Barhoun, H. El Ghallali, S. Borensztjan, F. Lantelme, Study of electrochemical reduction of $Zr^{4+}$ ions in molten alkali fluorides, Journal of the Electrochemical Society 155 (2008) E19.
[9] F.R. Clayton, G. Mamantov, D.L. Manning, Electrochemical studies of uranium and thorium in molten LiF–NaF-KF at 500°C, Journal of the Electrochemical Society 121 (1974) 86.
[10] C. Hamel, P. Chamelot, A. Laplace, E. Walle, O. Dugne, P. Taxil, Reduction process of uranium(IV) and uranium(III) in molten fluorides, Electrochimica Acta 52 (2007) 3995.
[11] P. Soucek, L. Cassayre, R. Malmbeck, E. Mendes, R. Jardin, J.-P. Glatz, Electrorefining of U-Pu-Zr-alloy fuel onto solid aluminium cathodes in molten LiCl-KCl, Radiochimica Acta 96 (4–5) (2008) 315.
[12] O.S. Monnahela, B.M. Vilakazi, J.B. Wagener, A. Roodt, P.A.B. Carstens, W.L. Retief, A thermogravimetric study of the fluorination of zirconium and hafnium oxides with fluorine gas, Journal of Fluorine Chemistry 135 (2012) 246.
[13] B.M. Vilakazi, O.S. Monnahela, J.B. Wagener, P.A.B. Carstens, T. Ntsoane, A thermogravimetric study of the fluorination of zirconium and hafnium oxides with anhydrous hydrogen fluoride gas, Journal of Fluorine Chemistry 141 (2012) 64.
[14] V.V. Guzeev, A.N. D'yachenko, Autoclave breakdown of zircon with ammonium fluorides, Russian Journal of Applied Chemistry 79 (2006) 1757.
[15] P. Joubert, B. Gaudreau, Tetravalent zirconium oxyfluorides, Reviews on Mineral Chemistry 12 (1975) 289.
[16] R. Papiernik, B. Frit, B. Gaudreau, Les phases solides du système $ZrO_2-ZrF_4$ = Solid phases in $ZrO_2-ZrF_4$ system, Revue de Chimie Minérale 23 (1986) 400.
[17] S. Ghosh, S. Vandarkuzhali, P. Venkatesh, G. Seenivasan, T. Subramanian, B. Prabhakara Reddy, K. Nagarajan, Electrochemical studies on the redox behaviour of zirconium in molten LiCl-KCl eutectic, Journal of Electroanalytical Chemistry 622 (2009) 15.
[18] Z. Chen, Y.J. Li, S.J. Li, Electrochemical behaviour of zirconium in the LiCl-KCL molten salt at Mo electrode, Journal of Alloys and Compounds 509 (2011) 5958.
[19] Y. Wu, Z. Xu, S. Chen, L. Wang, G. Li, Electrochemical behavior of zirconium in molten NaCl-KCl-$K_2ZrF_6$ system, Rare Metals 30 (2011) 8.
[20] H.A. Wilhelm, K.A. Walsh, US Patent 2602725 (1952).
[21] G.W. Mellors, S. Senderoff, The electrodeposition of coherent deposits of refractory metals: III - zirconium, Journal of the Electrochemical Society 113 (1966) 60.
[22] G.W. Mellors, S. Senderoff, Electrodeposition of coherent coatings of refractory metals: VII - zirconium diboride, Journal of the Electrochemical Society 118 (1971) 220.
[23] G.J. Kipouros, S.N. Flengas, Electrorefining of zirconium metal in alkali chloride and alkali fluoride fused electrolytes, Journal of the Electrochemical Society 132 (1985) 1087.
[24] K.H. Stern, Electrodeposition of refractory carbide coatings from fluoride melts, Journal of Applied Electrochemistry 22 (1992) 717.
[25] H. Groult, A. Barhoun, E. Briot, F. Lantelme, C.M. Julien, Electrodeposition of Zr on graphite in molten fluorides, Journal of Fluorine Chemistry 132 (2011) 1122.
[26] P. Chamelot, P. Taxil, B. Lafage, Voltammetric studies of tantalum electrodeposition baths, Electrochimica Acta 39–17 (1994) 2571.
[27] A.D. Graves, D. Inman, Adsorption and the differential capacitance of the electrical double-layer at platinum/halide metal interfaces, Nature 208 (1965) 481.
[28] A.J. Bard, R.L. Faulkner, Electrochemistry: Principles, Methods and Applications, Wiley, New York, 1980.
[29] R.K. Jain, H.C. Gaur, B.J. Welch, Chronopotentiometry: a review of theoretical principles, Journal of Electroanalytical Chemistry 79 (1977) 211.
[30] P. Chamelot, B. Lafage, P. Taxil, Using square-wave voltammetry to monitor molten alkaline fluoride baths for electrodeposition of niobium, Electrochimica Acta 43 (1997) 607.
[31] L. Ramalay, M.S. Kraus, Theory of square wave voltammetry, Analytical Chemistry 41 (1969) 1362.
[32] C. Hamel, P. Chamelot, P. Taxil, Neodymium(III) cathodic processes in molten fluorides, Electrochimica Acta 49 (2004) 4467.
[33] P. Taxil, L. Massot, C. Nourry, M. Gibilaro, P. Chamelot, L. Cassayre, Lanthanides extraction processes in molten fluoride media: Application to nuclear spent fuel reprocessing, Journal of Fluorine Chemistry 130 (2009) 94.
[34] R. Bormann, F. Gartner, F. Haider, Determination of the free energy of equilibrium and metastable phases in the Cu-Zr system, Materials Science and Engineering 97 (1988) 79.
[35] L. Bsenko, The Hf-Ni and Zr-Ni systems in the region 65-80 at.% Ni, Journal of the Less Common Metals 63 (1979) 171.
[36] A. Brenner, Electrodeposition of Alloys: Principles and Practice, vol. 1, Academic Press, New York, 1963.
[37] M. Gibilaro, L. Massot, P. Chamelot, P. Taxil, Electrochemical preparation of aluminium–nickel alloys by under-potential deposition in molten fluorides, Journal of Alloys and Compounds 471 (2009) 412.
[38] P. Taxil, Formation d'alliages tantale-nickel par voie électrochimique, Journal of the Less Common Metals 113 (1985) 89.
[39] C. Nourry, L. Massot, P. Chamelot, P. Taxil, Electrochemical reduction of Gd(III) and Nd(III) on reactive cathode material in molten fluoride media, Journal of Applied Electrochemistry 39 (2009) 927.
[40] Database from Scientific Group Thermodata Europe (SGTE), <http://www.sgte.org>.